remote sensing

Article

Advancing Forest Inventory in Tropical Rainforests: A Multi-Source LiDAR Approach for Accurate 3D Tree Modeling and Volume Estimation

Zongzhu Chen [1,2,*], Ziwei Lin [3,4], Tiezhu Shi [3,4], Dongping Deng [3,4], Yiqing Chen [1,2], Xiaoyan Pan [1,2], Xiaohua Chen [1,2], Tingtian Wu [1,2], Jinrui Lei [1,2] and Yuanling Li [1,2]

[1] Hainan Academy of Forestry, Haikou 571100, China; yiqingchen@hnaf.ac.cn (Y.C.); panxiaoyan@hnaf.ac.cn (X.P.); xiaohuachen@hnaf.ac.cn (X.C.); tingtianwu@hnaf.ac.cn (T.W.); jinruilei@hnaf.ac.cn (J.L.); yuanlingli@hnaf.ac.cn (Y.L.)
[2] Key Laboratory of Tropical Forestry Resources Monitoring and Application of Hainan Province, Haikou 571100, China
[3] State Key Laboratory of Subtropical Building and Urban Science & Key Laboratory for Geo-Environmental Monitoring of Coastal Zone of the National Administration of Surveying, Shenzhen University, Shenzhen 518060, China; linziwei2019@email.szu.edu.cn (Z.L.); tiezhushi@szu.edu.cn (T.S.); 2100325021@email.szu.edu.cn (D.D.)
[4] School of Architecture & Urban Planning, Shenzhen University, Shenzhen 518060, China
* Correspondence: zongzhu.chen@hnaf.ac.cn

Abstract

This study proposes an Automatic Branch Modeling (ABM) framework that combines AdTree and AdQSM algorithms to reconstruct individual tree models and estimate timber volume from fused Hand-held Laser Scanners (HLS) and Unmanned Aerial Vehicle Laser Scanners (UAV-LS) point cloud data. The research focuses on two 50 × 50 m primary tropical rainforest plots in Hainan Island, China, characterized by dense and vertically stratified vegetation. Key steps include multi-source point cloud registration and noise removal, individual tree segmentation using the Comparative Shortest Path (CSP) algorithm, extraction of diameter at breast height (DBH) and tree height, and 3D reconstruction and volume estimation via cylindrical fitting and convex polyhedron decomposition. Results demonstrate high accuracy in parameter extraction, with DBH estimation achieving R^2 = 0.89–0.90, RMSE = 2.93–3.95 cm and RMSE% = 13.95–14.75%, while tree height estimation yielded R^2 = 0.89–0.94, RMSE = 1.26–1.81 m and RMSE% = 9.41–13.2%. Timber volume estimates showed strong agreement with binary volume models (R^2 = 0.90–0.94, RMSE = 0.10–0.18 m^3, RMSE% = 32.33–34.65%), validated by concordance correlation coefficients (CCC) of 0.95–0.97. The fusion of HLS (ground-level trunk details) and UAV-LS (canopy structure) data significantly improved structural completeness, overcoming occlusion challenges in dense forests. This study highlights the efficacy of multi-source LiDAR fusion and 3D modeling for precise forest inventory in complex ecosystems. The ABM framework provides a scalable, non-destructive alternative to traditional methods, supporting carbon stock assessment and sustainable forest management in tropical rainforests. Future work should refine individual tree segmentation and wood-leaf separation to further enhance accuracy in heterogeneous environments.

Keywords: LiDAR fusion; tropical rainforest; 3D reconstruction; individual tree volume; AdQSM

check for updates

Academic Editors: Panagiotidis Dimitrios and Arturo Sanchez-Azofeifa

Received: 17 May 2025
Revised: 25 August 2025
Accepted: 27 August 2025
Published: 1 September 2025

Citation: Chen, Z.; Lin, Z.; Shi, T.; Deng, D.; Chen, Y.; Pan, X.; Chen, X.; Wu, T.; Lei, J.; Li, Y. Advancing Forest Inventory in Tropical Rainforests: A Multi-Source LiDAR Approach for Accurate 3D Tree Modeling and Volume Estimation. *Remote Sens.* **2025**, *17*, 3030. https://doi.org/10.3390/rs17173030

1. Introduction

Forest ecosystems serve as the cornerstone of terrestrial ecosystems and are pivotal to the biosphere, exerting a profound influence on the regulation of the global carbon cycle and the maintenance of climate stability [1]. Forest inventory efforts are instrumental in enabling precise and continuous monitoring of dynamic forest attributes, thereby supporting the formulation of effective forest management strategies. The paramount objective of forest surveys is to acquire detailed spatial structural parameters, encompassing metrics such as canopy height, leaf area index, diameter at breast height (DBH), tree height, and volumetric assessments. However, conventional forest survey methodologies are often hindered by prohibitive costs and time-intensive requirements [2], thereby substantially constraining the practicality of establishing long-term forest monitoring programs.

In recent years, the advancement of Light Detection and Ranging (LiDAR) technology, particularly its synergistic integration with unmanned aerial vehicles (UAVs) to pioneer UAV-LiDAR systems (UAV-LS), has unveiled remarkable advantages in the realm of forest surveys [3,4]. UAV-LS systems excel in swiftly capturing high-density, high-resolution 3D point cloud datasets within forested landscapes. This exceptional capability empowers the extraction of pivotal forest parameters, including tree height, crown spread, and stand density at the individual tree level across survey plots, thereby refining the precision of forest volume estimations [5,6]. Moreover, the integration of UAV-LS technology into forest inventory workflows significantly bolsters operational efficiency, streamlining processes and enhancing productivity.

Ground-based LiDAR systems, encompassing Terrestrial Laser Scanning (TLS) and Mobile Laser Scanning (MLS), offer the capability to scan forest interiors from the ground upwards, thereby capturing intricate spatial structural parameters with remarkable precision. These systems hold significant promise for accurately estimating forest timber volumes due to their ability to delineate fine-scale details within forested environments [7,8]. TLS, leveraging a stationary LiDAR platform, excels in generating highly accurate point cloud datasets of trees, and has found widespread application across diverse facets of forest surveys and parameter extraction [9–13]. However, the data acquisition process using TLS often demands substantial time investments and necessitates multiple scanner repositionings (or multi-station setups) to ensure comprehensive coverage of survey plots, which can be time-consuming and labor-intensive [14].

In contrast, MLS systems, including backpack laser scanning (BLS) and handheld laser scanning (HLS) configurations, enable seamless, continuous point cloud data collection while in motion. This capability facilitates the rapid acquisition of nearly complete plot datasets within significantly reduced timeframes, enhancing operational efficiency and data acquisition throughput. Recent research endeavors exploring the application of MLS technologies for extracting individual tree parameters in forestry surveys have reported encouraging preliminary findings, underscoring the potential of MLS systems to revolutionize forest inventory practices [15–17].

In practical forest inventory operations, acquiring comprehensive three-dimensional structural information using a solitary LiDAR device poses substantial challenges, particularly within complex ecosystems such as the tropical rainforests of Hainan Island, China. These environments are characterized by intricate vertical stratification and densely packed tree crowns with irregular, interwoven distributions, significantly complicating the task of achieving thorough data capture. For example, while UAV-LiDAR systems (UAV-LS) excel at capturing detailed information pertaining to forest canopy height, they often fall short in recording critical trunk-level details due to the limited penetration capacity of laser beams through dense foliage [18]. Conversely, ground-based LiDAR systems are adept at obtaining high-resolution point clouds of tree trunks and understory features, yet they encounter difficulties in capturing structural information from the upper canopy layers [19].

These inherent constraints associated with single-source LiDAR data collection lead to incomplete point cloud datasets, thereby introducing considerable inaccuracies in the measurement of forest structural parameters and subsequent timber volume estimations. As a result, the integration of multisource remote sensing data has emerged as an indispensable strategy for achieving comprehensive and precise measurements of forest 3D structure. This synergistic approach leverages the complementary strengths of diverse data sources to mitigate the limitations of individual sensors, ultimately enhancing the accuracy and reliability of forest inventory assessments [20].

In recent years, Quantitative Structure Models (QSM) algorithms have gained prominence for their capacity to non-destructively estimate tree volume through three-dimensional simulations that replicate the actual morphological characteristics of individual trees [16,21,22]. This innovative methodology has found significant application in tropical forest research, where it facilitates detailed volumetric assessments without the need for invasive sampling techniques. For instance, Tanago et al. [23] leveraged Terrestrial Laser Scanning (TLS) point clouds to construct intricate 3D tree models, thereby enabling the estimation of aboveground biomass in large tropical forest trees. Their study underscored the efficacy of QSM algorithms in navigating the complex structural configurations inherent to tropical forest ecosystems. Similarly, Krishna Moorthy et al. [24] employed the TLS-QSM framework to estimate the volume of liana stems within tropical forests, revealing a robust correlation between volumes derived from 3D tree models and those obtained through direct measurements.

Building upon these advancements, Du et al. [25] and Fan et al. [26] introduced the AdTree and AdQSM methodologies, which further expanded the capabilities of QSM algorithms. These approaches provide a robust geometric foundation for automated, high-fidelity, and precise 3D reconstructions of actual trees, while simultaneously enabling the quantification of key forest inventory parameters such as diameter at breast height (DBH), tree height, and volume. The accuracy of the AdQSM method in estimating individual tree attributes—including DBH, height, volume, and aboveground biomass (AGB)—has been rigorously validated across diverse datasets, encompassing LiDAR point clouds, photogrammetric point cloud data, and even destructive sampling data [27]. These validations underscore the reliability and versatility of AdQSM in addressing the complexities of forest inventory tasks across a range of environmental conditions.

However, a notable limitation of these existing methodologies is their exclusive reliance on singular LiDAR data sources, without incorporating the fusion of terrestrial and aerial datasets. This constraint is particularly pronounced in structurally intricate tropical rainforests, where a single data source often proves inadequate in capturing the full spectrum of forest structural information. The integration of data from multiple perspectives—encompassing both ground-based and aerial vantage points—is therefore imperative to enrich the dataset and enhance the accuracy and comprehensiveness of forest structural assessments. Moreover, the AdQSM algorithm, while advanced, does not inherently incorporate a wood-leaf separation step within its processing pipeline. In tropical rainforests, trees are typically characterized by luxuriant foliage with complex and heterogeneous spatial distributions. This dense and variable canopy cover can significantly confound modeling outcomes, as the algorithm may struggle to differentiate between woody components and foliage when reconstructing tree structures from point cloud data [28]. Consequently, implementing a preprocessing step for wood-leaf separation is essential to ensure that the subsequent reconstruction of woody components is based on accurate and uncontaminated point cloud data, thereby yielding more reliable and precise results.

The tropical rainforests of Hainan Island serve as China's equatorially nearest rainforest ecosystem, forming a cornerstone of the nation's rainforest biome. Despite constituting only 22% of the world's potential vegetation area [29], these rainforests are disproportionate carbon sinks, storing 59% of global forest carbon and thereby playing a pivotal role in modulating the global carbon balance and sustaining climate stability [30]. In the context of escalating global concerns over carbon neutrality and climate change, the precise estimation of tree volume within this region is imperative. Such accuracy is vital for elucidating Hainan Island's carbon sequestration potential and for assessing the integral role that Chinese tropical rainforest ecosystems play within the broader global carbon cycle.

This study concentrates on rainforest sample plots situated within Hainan Island, employing an innovative fusion of Handheld Laser Scanning (HLS) and Unmanned Aerial Vehicle-based Laser Scanning (UAV-LS) point cloud datasets to meticulously extract individual tree structural parameters, notably diameter at breast height (DBH) and tree height. The research methodology synergistically integrates advanced wood-leaf separation techniques with the sophisticated AdQSM algorithm to facilitate precise estimation of individual tree volumes. The research objectives are three-pronged: (1) to amalgamate HLS and UAV-LS LiDAR data, thereby enabling the extraction of individual tree parameters within the intricate structural matrices of Hainan Island's tropical rainforest stands; (2) to construct detailed individual tree models by integrating wood-leaf separation methodologies with the AdQSM algorithm, with the specific aim of enhancing the accuracy of tree volume estimations; (3) to critically evaluate the feasibility of the proposed methodology by juxtaposing the modeled individual tree volumes against those derived from established binary volume models, thereby ascertaining the method's efficacy and reliability. This integrated framework is rigorously validated through meticulous comparisons with field-measured data, ensuring the robustness and reliability of the findings.

2. Materials

2.1. Forestry Data Acquisitions

The research area is situated within the Hainan Island Tropical Rainforest National Park (Figure 1), renowned for its exceptional biodiversity and ecological significance. Within this expansive protected area, forest coverage attains an impressive 95.86%, underscoring its status as a vital ecological haven. Natural forests dominate the landscape, spanning 3267.93 km^2 and constituting 76.56% of the national park's total area. Plantation forests, though smaller in scale, cover 824 km^2 and account for 19.3% of the park's territory, contributing to the region's diverse forest mosaic. The park is situated within a tropical marine monsoon climate zone, characterized by abundant sunshine and high total solar radiation, which foster a year-round warm and humid environment. The annual average temperature oscillates between 22.5 °C and 26.0 °C, creating a conducive microclimate for tropical flora and fauna. Precipitation is equally generous, with an annual average rainfall of 1759 mm, ensuring a lush and verdant ecosystem.

For the purposes of this study, we selected two 50 $\times$ 50 m primary forest plots as our research sites. Given the study's focus on quantifying the standing timber volume within these plots, we meticulously measured the DBH and tree height for all trees within the sample plots. These measurements, summarized in Table 1, provide a detailed snapshot of the forest's structural attributes. By leveraging advanced remote sensing technologies and rigorous field measurements, this study seeks to enhance our understanding of forest carbon dynamics and inform sustainable forest management practices in Hainan's tropical rainforests.

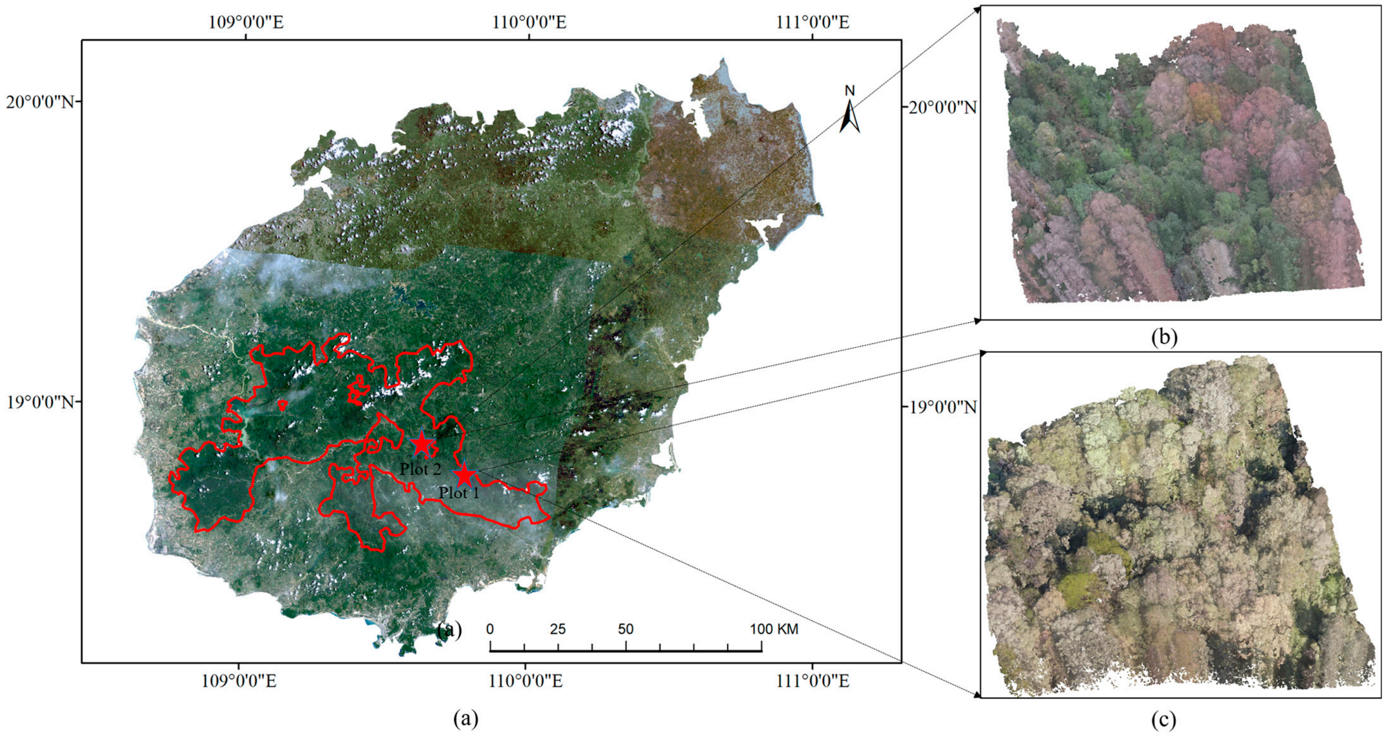

Figure 1. Schematic diagram of study area and sample plot. (**a**) Hainan Island Tropical Rainforest National Park (red border) and red stars represent the locations of two plots; (**b**) schematic diagram of plot 2; (**c**) schematic diagram of plot 1.

Table 1. Field survey structural data of sample plots.

Plot	Tree Count	DBH (cm)			Tree Height (m)		
		Average	Min	Max	Average	Min	Max
1	109	21.00	8.14	51.6	13.43	5.069	21.75
2	97	26.78	7.8	75.16	13.73	3.283	28.658

Note: Tree count is total number of trees measured in each plot. DBH is the diameter at breast height, Min is Minimum, Max is maximum.

2.2. Handheld Laser Scanning Data

The HLS data for this study were collected on 15 December 2024, under optimal conditions of clear weather and moderate afternoon breeze (2:00–2:45 p.m.) to ensure high-fidelity 3D point cloud acquisition. The Feima SLAM100 handheld laser scanner (Feima Robotics Co., Ltd., Shenzhen, China), featuring a 360° rotating head, light-independent operation, and SLAM-based GPS-free navigation, was deployed to capture the 50 × 50 m sample plots with 5 cm absolute accuracy and a 120 m max measurement range. Scanning each plot required approximately 25 min, including initialization, structured grid-like paths with overlapping coverage, and real-time quality checks via the SLAM Go APP, followed by 10 min of post-processing for data registration and export. The resulting point cloud for plot 1 (Figure 2a) demonstrates dense reconstruction of tree trunks, understory vegetation, and ground topography with minimal occlusion artifacts, validating the SLAM100's suitability for complex tropical rainforest environments and providing a robust foundation for subsequent wood-leaf separation, tree segmentation, and volume estimation analyses.

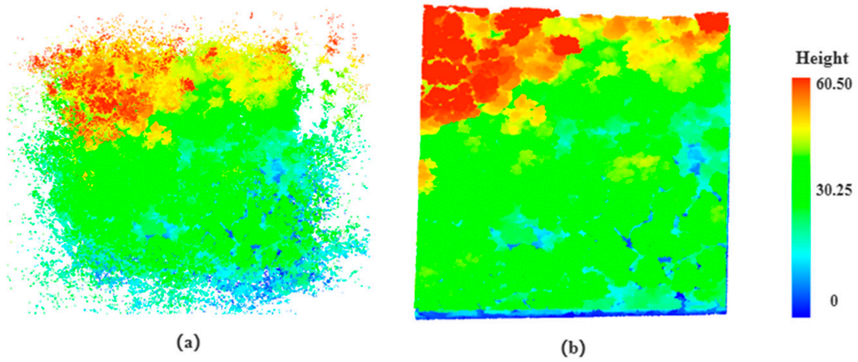

Figure 2. The point cloud data of plot1, (**a**) The point cloud data acquired by Feima SLAM100 handheld laser scanner; (**b**) The point cloud data acquired by DJI UAV combined with Zenith L2 equipment.

2.3. UAV-LS Data

The UAV-LiDAR data were acquired using a DJI M300 RTK multi-rotor UAV (Da-Jiang Innovations Science and Technology Co., Ltd., Shenzhen, China) paired with a Zenith L2 LiDAR sensor (Da-Jiang Innovations Science and Technology Co., Ltd., Shenzhen, China), chosen for its robust performance in challenging tropical rainforest environments. The UAV's integrated RTK module ensures sub-centimeter geospatial accuracy ($\leq$10 mm + 1 ppm horizontal, $\leq$15 mm + 1 ppm vertical), critical for aligning LiDAR returns with ground control points and HLS datasets. The Zenith L2 sensor operates efficiently across a −20 °C to 50 °C temperature range and achieves a maximum point cloud data rate of 1.2 million points/s under multi-echo conditions, enabling rapid and dense 3D reconstruction. At a 150 m relative flight altitude, the system achieves $\leq$5 cm planar accuracy and $\leq$4 cm elevation accuracy, facilitating detailed topographic and canopy structure mapping. To maximize ground point extraction in dense vegetation, flights were conducted at 100 m altitude with a 5-echo maximum setting, balancing penetration depth and data density.

UAV missions were timed to coincide with handheld LiDAR (HLS) surveys to ensure temporal consistency. Flight plans were pre-programmed using DJI Terra (V4.2.5) software, optimizing route overlap (70%) and scan angle (±15° from nadir) for uniform coverage. Each 50 × 50 m sample plot required 15 min for data collection, including system initialization, automated flight execution, and real-time monitoring via the DJI Pilot 2 app. Post-processing with DJI Terra (V4.2.5) software involved: (1) RTK-corrected trajectory alignment to minimize drift, (2) multi-echo point cloud classification to separate ground and vegetation returns, and (3) noise filtering to remove atmospheric artifacts. This workflow yielded a high-precision point cloud dataset in ~30 min per plot, ensuring seamless integration with HLS data for multi-sensor fusion.

3. Methods

The overall workflow of this study is shown in the Figure 3 below. Initially, the UAV-LS and HLS datasets are fused. Subsequently, the fused point cloud data is segmented to extract individual tree-level point clouds. In the final stage, individual tree models are constructed and relevant parameters are extracted.

3.1. Point Cloud Registration and Noise Removal

To achieve a seamless and multi-scale representation of forest structure, the integration of HLS and UAV-LS point clouds was anchored in a GNSS-centric registration framework during data acquisition, ensuring both datasets were inherently aligned to the China Geodetic Coordinate System 2000 (CGCS2000). For UAV-LS data, the DJI M300 RTK's IMU-GNSS (Da-Jiang Innovations Science and Technology Co., Ltd., Shenzhen, China) integration provided RTK corrections, achieving sub-centimeter horizontal accuracy (<1 cm) and vertical precision (<1.5 cm) by fusing inertial measurements with satellite-derived positions. This system captured dense canopy returns while anchoring trajectories to the CGCS2000 grid. For HLS data, the Feima SLAM100 scanner (Feima Robotics Co., Ltd., Shenzhen, China) combined SLAM-based pose estimation with intermittent GNSS fixes (when canopy gaps permitted), enabling ground-level structural mapping with 5 cm absolute accuracy. The dual-GNSS approach ensured that both datasets shared a common coordinate reference, eliminating the need for post-hoc spatial transformations and minimizing registration errors.

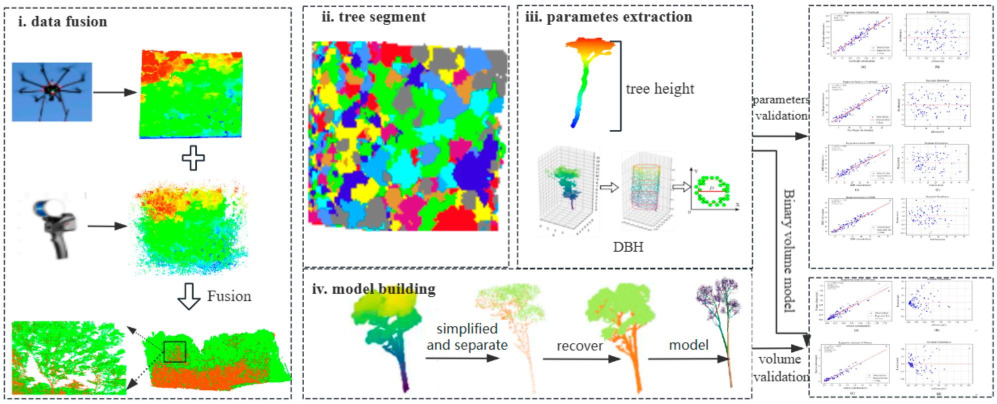

Figure 3. Overview of the research workflow.

The CloudCompare platform [31] was employed for final validation and fusion of the datasets, leveraging iterative algorithms to refine alignment. Key steps included: (1) coarse alignment verification using common control points (e.g., plot boundaries, exposed ground markers) to confirm sub-meter agreement; (2) Iterative Closest Point (ICP) [32] optimization to minimize point-to-point distances in overlapping regions, achieving registration RMSE values < 10 cm; and (3) quality checks via visual inspection of canopy-ground continuity and statistical analysis of point density distributions. The resulting merged point cloud (Figure 4) fused dense UAV-LS canopy returns (e.g., leaf area density, crown shape) with detailed HLS ground-level data (e.g., stem diameters, understory biomass), enabling holistic analysis of forest vertical structure. The schematic in Figure 4 illustrates the seamless overlay of HLS (red) and UAV-LS (green) datasets, demonstrating <10 cm registration accuracy in overlapping zones and highlighting the synergy between airborne and terrestrial LiDAR systems for tropical rainforest structural monitoring. This workflow ensures methodological rigor, supporting robust carbon stock estimation and ecological research in complex forest ecosystems.

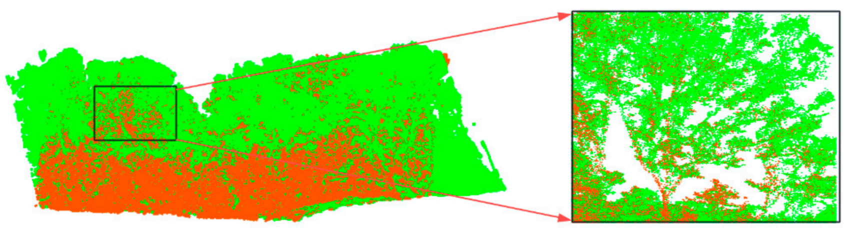

Figure 4. Schematic diagram of fused HLS and UAV-LS point cloud data. Red represents HLS data, green represents UAV-LS data (The image on the right is an enlarged view of the black box on the left).

After data registration, the aligned data underwent resampling to reduce the point cloud data volume and eliminate some noise points. A random downsampling method was initially employed to reduce the number of points by specifying a sampling rate.

Considering the high point density in the study area, a sampling rate of 10% was adopted in this study based on the results of multiple experimental trials. Subsequently, a statistical filtering method [32] was applied to the resampled data to remove noise points. This method calculated the mean (μ) and standard deviation (σ) of global distances, treating neighboring points outside the interval defined by the mean and standard deviation ($\mu \pm 3\sigma$) as noise. This method effectively removed isolated outliers while preserving critical structural details such as fine branches and understory vegetation. After resampling and noise removal, the number of points was reduced to approximately 30 million for plot 1 and 37 million for plot 2. The optimized dataset provides a computationally efficient foundation for subsequent individual tree segmentation, modeling, and volume estimation in the Hainan tropical rainforest.

3.2. Feature Parameters Extraction

The CSP point cloud segmentation algorithm [33] is used to segment the registered point cloud into individual trees before parameter extraction. The CSP algorithm employs the shortest path approach and the theory of metabolic ecology, which can effectively address the individual tree segmentation problem under various forest conditions with strong adaptability and robustness.

The CSP method initially identifies seed points at the base of tree trunks, then proceeds with individual tree segmentation based on these seed points. The presence of low shrubs within the sample plot can significantly affect seed point extraction accuracy. Therefore, during seed point acquisition, we strategically elevated the position of seed point extraction to minimize interference from low vegetation. Furthermore, following the automated individual tree segmentation process, any remaining shrubs and vines that could not be automatically filtered were manually removed from the dataset. It is important to note that the CSP algorithm requires normalization of the sample plot based on ground point elevations. Ground point identification was accomplished using an improved progressive triangulated irregular network (TIN) filtering algorithm [34]. Subsequently, point cloud normalization was achieved by subtracting the Digital Elevation Model (DEM) height values from the corresponding point cloud height values.

During the individual tree segmentation process using the CSP algorithm, key parameters were set to enhance segmentation accuracy: the minimum number of clustering points was set to 500, the minimum tree height to 3 m, and the trunk height to 2 m. These thresholds were selected to reduce interference from low-lying shrubs and non-tree vegetation. The algorithm initially extracted approximately 1000 individual tree point clouds from both plot 1 and plot 2. However, the raw results included substantial noise and numerous small-sized plants. After manual screening and the exclusion of trees with a DBH less than 7 cm, a total of 109 individual tree point clouds were retained for plot 1 and 97 for plot 2.

DBH and Tree Height (H_t) Acquisition

After completing individual tree segmentation, the next pivotal step entailed extracting pertinent parameters, namely the DBH and tree height. To mitigate the impact of local shape irregularities and gaps in the point cloud data on measurement accuracy, we began by isolating two distinct horizontal slices from each individual tree's point cloud. These slices were positioned at heights of 1.0–1.15 m and 1.25–1.40 m, respectively. For trees exhibiting a divergent base structure, the slice heights were judiciously adjusted downward following a manual selection process. Once the slices were extracted, they were projected onto the XY plane. A least-squares circle fitting algorithm was then applied to these projections to determine the best-fit circles. Subsequently, the diameters corresponding to these circles were calculated. The final DBH value for each tree was obtained by averaging the diameters derived from the two projected point cloud slices. It is worth noting that the least-squares circle fitting method is widely regarded as one of the most precise techniques for DBH extraction, outperforming alternatives such as the Hough transform circle detection and cylinder fitting algorithms, as evidenced by reference [16]. A schematic diagram illustrating the DBH acquisition process is presented in Figure 5 below.

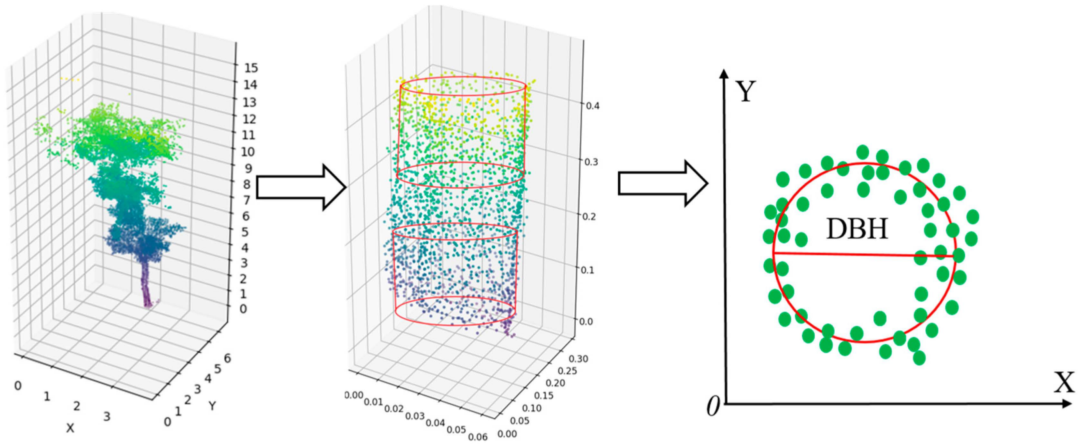

Figure 5. Simulation of DBH extraction (the image is generated by the Python (v3.10) matplotlib library (v3.5.0)). On the left is a demonstration image of a single tree point cloud, with a fitted cylinder in the middle (red) and a top view on the right, with the fitted circle in red.

In this research, we registered the point cloud data with both the HLS point cloud and the UAV-LS point cloud. This integration facilitated a more comprehensive representation of each individual tree's morphology. Furthermore, prior to analysis, the plot point cloud data underwent a normalization process. Consequently, the tree height for each individual in our study was defined as the maximum value of the Z-coordinate component within its respective point cloud. Mathematically, this can be expressed using the following formula:

$$\boldsymbol{H_t} = \boldsymbol{Z_{max}} \quad (1)$$

Here, H_t denotes the tree height of the individual tree, and Z_{max} denotes the maximum value of the Z component of individual tree point cloud in the point cloud coordinate.

3.3. Model Construction and Volume Calculation

3.3.1. Automatic Branch Modeling (ABM)

The ABM approach for tree structure analysis comprises four principal stages, as visually outlined in Figure 6. The initial step involves the segmentation of individual trees from the registered point cloud data, a process that has been elaborated upon in prior sections. The second stage focuses on extracting branch points and deriving the skeletal structure from the point cloud data corresponding to each individual tree. This step is crucial for understanding the branching pattern and overall architectural framework of the tree. In the third phase, we employ a segmented cylinder fitting technique on the branch point cloud to construct a detailed trunk model. This modeling is achieved through the integration of the AdTree and AdQSM algorithms, which together offer a sophisticated and adaptable approach to capturing the trunk's geometric intricacies. Finally, the fourth step involves calculating volume statistics for the fitted cylindrical sections of each individual tree's trunk. These volume measurements serve as the basis for estimating the timber volume of each tree, a key metric in forestry and ecological assessments. The subsequent sections of this discourse will predominantly center on the methodologies and outcomes associated with Steps 2, 3, and 4, providing in-depth insights into the technical procedures and analytical findings.

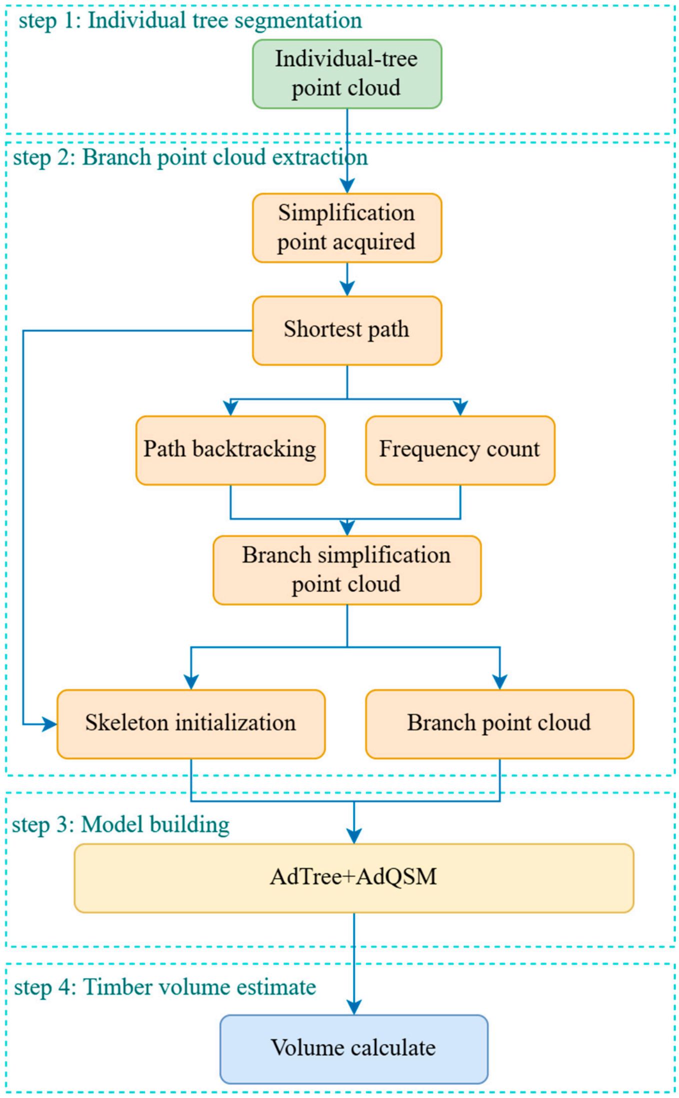

Figure 6. Flowchart for timber volume estimation using ABM.

3.3.2. Branch Point Cloud Segmentation

Given the sheer volume and inherent complexity of raw point cloud data, this study employs a preprocessing strategy to streamline the dataset, thereby reducing noise and computational burden. Initially, we construct a KDTree from the original point cloud data of each individual tree. This spatial indexing structure is instrumental in optimizing subsequent search perations. We then identify the point with the lowest Z component value within the tree's point cloud, which serves as our starting reference point (i.e., the point located at the lowest position on the trunk). Leveraging the radius nearest-neighbor search method, we locate points within a predefined radius of this reference point. Taking into account the typical spacing between branches and leaves, as well as our objective to minimize point cloud complexity, we set the search radius to 0.1 m. Once the points within the specified radius are identified, we compute the mean coordinates of these points. This mean point effectively encapsulates the structural essence of the cluster, acting as a simplified representative. Following this, we eliminate the original point cloud cluster from our dataset to reduce computational overhead. We repeat this simplification process iteratively, progressing from the base of the tree upwards. Ultimately, we obtain a simplified point cloud dataset that captures the complete morphology of the individual tree with reduced complexity and noise. Mathematically, the simplified point expression is as follows:

$$\boldsymbol{C} = \frac{1}{\boldsymbol{n}} \sum_{\boldsymbol{i}=1}^{\boldsymbol{n}} \boldsymbol{c_i} \tag{2}$$

where, C represents the coordinates of the simplified point, and n represents the number of neighboring points searched through the radius nearest neighbor search mothed.

When the simplified points are determined, the well-known Dijkstra shortest path algorithm is used to calculate the shortest paths from the start point to other points in the individual tree point cloud. Then the individual tree branch points will be extracted based on the following two conditions:

(1) For each shortest path, seed points that exclude the start and end points are obtained from the points on the path. Generally, the distance from the start point to a branch point on the same shortest path is less than the distance from the start point to a leaf point. Therefore, a radius nearest-neighbor search is employed to find neighboring points near each seed point. Subsequently, the shortest paths from the start point to the seed point and from the start point to its neighboring points are determined. If the distance of the former is greater than the latter, the neighboring point is added to the set of non-leaf points. Based on this condition, a portion of the leaf points can be eliminated.

$$\begin{cases} \boldsymbol{p_i} \in \{\boldsymbol{non-leaf}\},\ \boldsymbol{if\ dis}(\boldsymbol{begin}, \boldsymbol{p_i}) < \boldsymbol{dis}\left(\boldsymbol{begin}, \boldsymbol{p_i^{seed}}\right) \\ \boldsymbol{p_i} \in \{\boldsymbol{other}\},\ \boldsymbol{otherwise} \end{cases} \tag{3}$$

p_i represents the neighboring points of the seed points p_i^{seed}, $dis(begin, p_i)$ and $dis\left(begin, p_i^{seed}\right)$ represents the shortest path distance from the start point to the neighboring points and seed point, respectively.

(2) Branch points characteristically exhibit high visit frequency in the shortest paths from the root start point to t various leaf points. By leveraging this distinctive feature, we record the traversal frequency of each point during shortest path calculations. Through comparative analysis of these frequency values, we can effectively distinguish branch points from other point types.

$$\begin{cases} \boldsymbol{p_i} \in \{\boldsymbol{wood}\},\ \boldsymbol{iflog}(\boldsymbol{freq}(\boldsymbol{p_i})) \geq \boldsymbol{\sigma} \cdot \boldsymbol{log}(\boldsymbol{max}(\boldsymbol{freq}(\boldsymbol{p}))),\ \boldsymbol{i} = \mathbf{1}, \mathbf{2}, \mathbf{3} \ldots, \boldsymbol{n} \\ \boldsymbol{p_i} \in \{\boldsymbol{other}\},\ \boldsymbol{otherwise} \end{cases} \tag{4}$$

p_i represents the points in the point cloud of individual tree, $freq(p_i)$ represents the access frequency of point p_i, σ is the set threshold, $log(max(freq(p)))$ denotes the logarithmic value of the highest value of the access frequency in the point cloud, and n represents the number of point clouds.

Following the application of the aforementioned filtering conditions, both simplified branch points and optimized shortest paths are obtained. Subsequently, these simplified branch points are used to recover the corresponding points from the original point cloud, resulting in the complete branch point cloud of the individual tree. This recovery process ensures that while the identification method leverages simplified representations for efficiency, the final branch point cloud maintains fidelity to the original data structure (Figure 7).

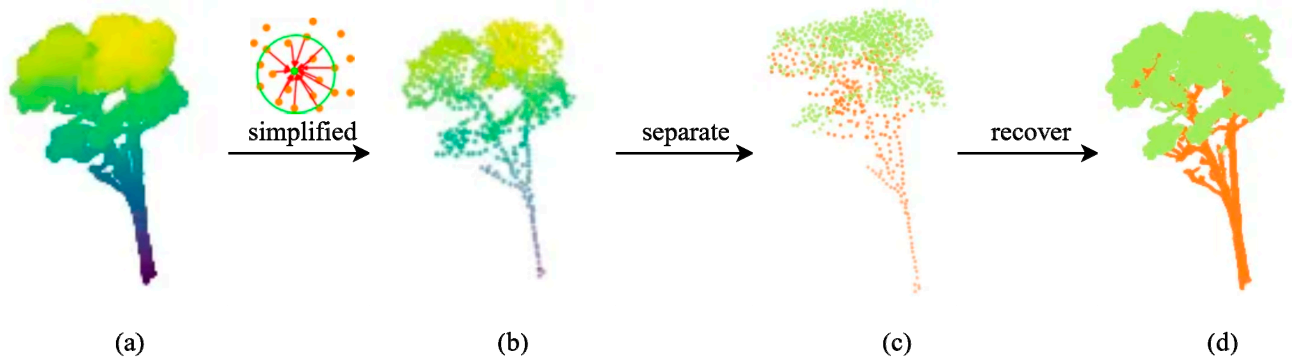

Figure 7. Schematic diagram of simplified point and branch and leaf separation. (**a**) Original tree point cloud; (**b**) simplified tree structure; (**c**) simplified point cloud after branch-leaf separation (Green represents leaves, orange represents branches); (**d**) reconstructed point cloud with separated branches and leaves(Green represents leaves, orange represents branches).

3.3.3. Model Building and Volume Estimation

Following branch point cloud segmentation, the shortest path of simplified branch points is derived, establishing the initial skeleton for model construction. With both the initial skeleton and branch point clouds available, trunk modeling proceeds using cylindrical fitting techniques as referenced in the AdTree approach. AdTree is a precise, automated modeling methodology that achieves tree model construction from laser-scanned data through point cloud segmentation and cylindrical fitting (Figure 8). The modeling process follows this sequence: initially, beginning at the tree trunk's root, a branch point cloud segment of predetermined height is extracted, after which a cylinder is fitted using iterative nonlinear least squares to accurately simulate the actual trunk morphology based on this point cloud segment. Subsequently, for upper branch sections with sparse point clouds, allometric growth rules [35] are applied to determine the radius of the fitted cylinder. Figure 8 illustrates the model construction process, while Figure 9 displays selected modeling results. The radius estimation is determined by the following expression:

$$r_c = r_p \times \left(\frac{l_c}{l_p}\right)^{\gamma} \tag{5}$$

where, r_c is the radius of current node, r_p represents the radius of its parent node, l_c and l_p is the total branch length supported by the current node and parent node. γ denotes the radius coefficient.

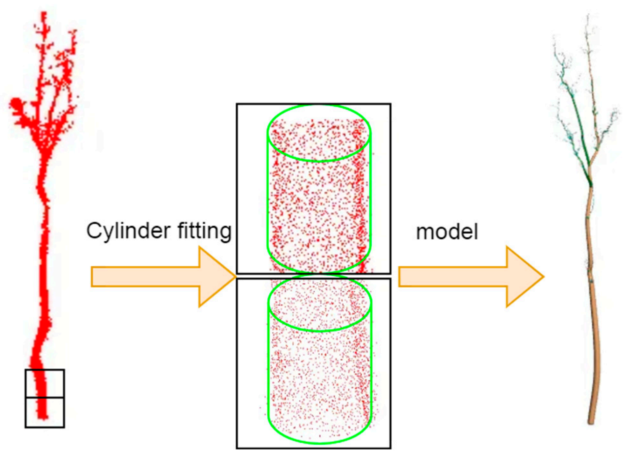

Figure 8. Model construction diagram, the point cloud in the black box is finally fitted as a green cylinder.

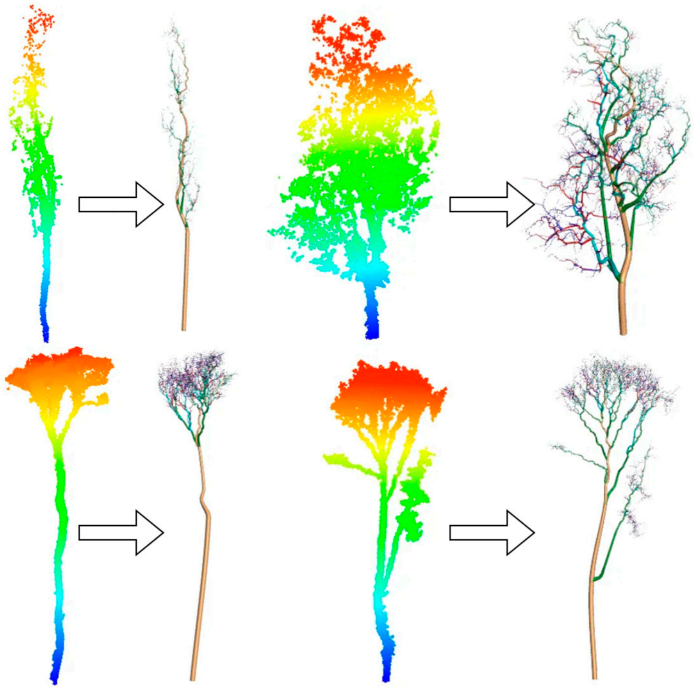

Figure 9. Tree modeling based on the ABM algorithm.

Following the completion of cylinder fitting, the entire individual tree model forms a complete and closed convex polyhedron. The tree volume calculation is performed using the method from AdQSM, with the volume calculation expression as follows:

$$\boldsymbol{volume} = \sum_{i=1}^{m}\sum_{j=1}^{n}\left(\frac{|(\boldsymbol{p}\times\boldsymbol{q})\cdot\boldsymbol{r}|}{6}\right) \tag{6}$$

where volume represents the total volume including both trunk and branches, m denotes the number of all convex polyhedra constituting the tree model, and n represents the number of all triangular pyramids forming the convex polyhedron. The variables p, q, and r represent the three vectors passing through the vertices of the triangular pyramid.

3.4. Validation

In order to evaluate the performance of the ABM method, this paper evaluates the accuracy of both individual tree parameters and individual tree volume estimation. The true value of individual tree volume is calculated using the formula of the binary volume model with the following expression:

$$V = \boldsymbol{f}\boldsymbol{D}^2\boldsymbol{H_t} \tag{7}$$

where V denotes the volume of the individual tree, D denotes the DBH of the individual tree, H_t denotes the height of an individual tree, f is the fitting parameter. According to the paper of Cheng et al. [36]. f differ between tree species and regions, the authors conducted numerous data experiments on different tree species in different regions. As the study area is situated in southern China and the sample plots comprise both needle-leaved and broad-leaved trees, the needle-leaved model and the broad-leaved model for the southern region in the paper were employed for the calculation of individual tree volume in this study. The specific values of the f are presented in Table 2. The individual tree timber volume calculated by the binary volume model was used as the reference value and compared with that obtained by re-modeling the individual tree with the ABM method.

Table 2. Binary volume model parameters and related indicators.

Model	f	R^2	Sum of Squared Residuals (m^3)
needle-leaved	3.5606×10^{-5}	0.991	0.05
broad-leaved	3.4099×10^{-5}	0.993	0.04

Root Mean Squared Error (RMSE), Root Mean Squared Error Percentage (RMSE%) and Coefficient of Determination (R^2) were used to evaluate the accuracy of DBH, tree height and timber volume, the RMSE and R^2 were expressed as follows:

$$\boldsymbol{RMSE} = \sqrt{\frac{\sum_{i=1}^{n}\left(y_i - y_i^r\right)^2}{n}} \tag{8}$$

$$\boldsymbol{RMSE\%} = \frac{\boldsymbol{RMSE}}{\overline{y}} \tag{9}$$

$$\boldsymbol{R}^2 = 1 - \frac{\sum_{i=1}^{n}\left(y_i - y_i^r\right)^2}{\sum_{i=1}^{n}\left(y_i - \overline{y}\right)^2} \tag{10}$$

where n denotes the number of samples, y_i denotes the calculated value of the correlation parameter for the ith tree, y_i^r denotes the actual observed value of the correlation parameter for the ith tree, and $\overline{y}$ denotes the average of the actual observed values of the correlation parameter for all trees in the plot.

In addition to the RMSE and the R^2, the Concordance Correlation Coefficient (CCC) was employed to assess the timber volume estimated by the ABM method, as demonstrated in the following expression:

$$\boldsymbol{CCC} = \frac{2\rho\sigma_x\sigma_y}{\sigma_x^2 + \sigma_y^2 + \left(\mu_x - \mu_y\right)^2} \tag{11}$$

where ρ denotes the correlation coefficient, σ denotes the variance of the input data, and μ denotes the mean of the input data.

4. Results

4.1. Precision Analysis of Individual Tree Parameters

4.1.1. DBH Accuracy

Figure 10 presents a comparative analysis of DBH estimates derived from our methodology against their field-measured reference values in two distinct plots, alongside the corresponding residual distributions. The Y-axis in each plot represents the reference values, obtained through meticulous in-field manual measurements. In plot 1, the linear regression model examining the relationship between the extracted DBH and the reference values demonstrates exceptional accuracy. The R^2 for this model is 0.89, indicating a strong linear correlation. The slope of the fitted regression line is 0.98, suggesting minimal deviation from the ideal 1:1 relationship. Furthermore, the RMSE is 2.93 cm, and the RMSE% is 13.95%, reflecting a relatively low average discrepancy between the predicted and actual DBH values. As depicted in Figure 10b, the residuals (the differences between predicted and actual values) are confined within a narrow range of −6 cm to 6 cm. Notably, the estimation accuracy remains consistent across the full spectrum of tree sizes, with no evident pattern of error increasing or decreasing with DBH.

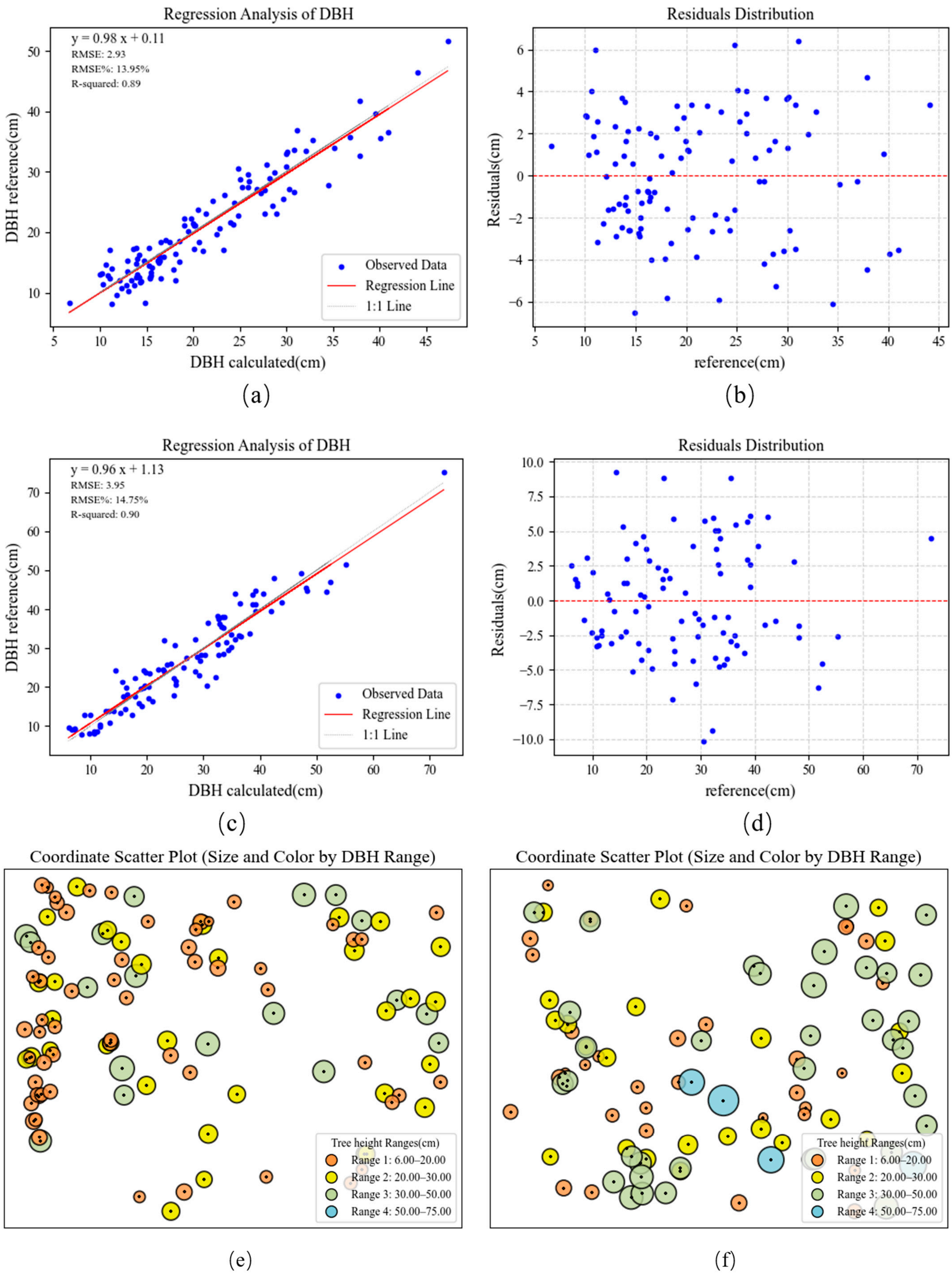

Figure 10. Comparison of extracted DBH values with field-measured reference data for two plots, and the distribution of calculated DBH for plot 1 (**e**) and plot 2 (**f**). (**a**,**b**) show the extracted DBH values versus the reference values and the corresponding residuals for plot 1; (**c**,**d**) present the same comparison for plot 2.

In plot 2, the linear regression model assessing the consistency between the extracted DBH and the reference values yields an R^2 of 0.90, still indicative of a robust linear relationship. The slope of the fitted line is 0.96, slightly lower than that of plot 1 but remaining close to the ideal. However, the RMSE in plot 2 is higher at 3.95 cm, the RMSE% is higher at 14.75%, and the residuals span a broader range of −10 cm to 10 cm, as illustrated in Figure 10d. This suggests that, while the model maintains a high level of accuracy, there is slightly greater variability in the DBH estimates compared to plot 1.

As shown in Table 1, the mean DBH of trees in plot 1 is 21 cm, whereas that in plot 2 is 26.78 cm. Combined with Figure 10f, trees in plot 2 generally exhibit larger DBH values than those in plot 1. Due to the complexity of the measurement environment and potential human measurement errors, larger tree diameters inherently introduce greater variability and measurement errors, potentially contributing to the higher RMSE and a relatively wider residual range for DBH measurements in plot 2. In plot 1, trees are more densely distributed and smaller in size, which may lead to denser foliage. Occlusion and overlapping branches can affect the quality of point cloud acquisition, thereby reducing the accuracy of DBH calculations. Overall, given the relatively large number of trees in both plots (109 in plot 1 and 97 in plot 2) and the application of the same estimation method, the difference in DBH estimation accuracy between the two plots is negligible, and both exhibit high estimation performance.

4.1.2. H_t Accuracy

Figure 11 presents a comparative assessment of tree height (H_t) estimates derived from individual tree point clouds against their field-measured reference values in two distinct plots, accompanied by the corresponding residual distributions. The linear regression analysis conducted on these datasets offers valuable insights into the accuracy and consistency of our height estimation methodology. In Figure 11a, the R^2 value for the relationship between extracted tree heights and reference values is 0.89, indicating a robust linear correlation. The slope of the fitted regression line is 0.93, closely approximating the ideal 1:1 relationship. The RMSE for this plot is 1.26 m, with a RMSE% of 9.41%, suggesting a low average deviation between predicted and actual tree heights. Similarly, in Figure 11c, the R^2 value is even higher at 0.94, with a fitted regression slope of 0.95. The RMSE is 1.81 m, and the RMSE% is 13.2%. These results underscore the high accuracy of tree height estimates obtained through our integrated approach, which leverages both HLS and UAV-LS point cloud data.

Examining the residual plots provides further nuance to these findings. In plot 1 (Figure 11b), the majority of tree height calculation residuals fall within a narrow range of −2 to 2 m, with only a few outliers beyond this interval. In contrast, plot 2 (Figure 11d) exhibits a slightly wider residual distribution, with most residuals ranging between −3 and 3 m and a few instances of larger discrepancies. Notably, higher residual values tend to occur in taller trees across both plots, likely due to the increased complexity and variability associated with measuring larger canopies. However, in plot 2, smaller trees also occasionally produce larger residuals, which may be attributed to data acquisition challenges.

As illustrated in Figure 11f, trees in sample plot 2 are generally taller than those in plot 1. According to Table 1, combined with the observation in Figure 10e, trees in plot 2 have larger DBH values, suggesting a potential occlusion effect. Larger and taller trees may obscure smaller ones, particularly in dense canopies, thereby impeding the collection of accurate UAV point cloud data for these smaller trees. This occlusion could contribute to the larger residuals observed in both taller and, in some cases, smaller trees within plot 2. Overall, the tree height estimations for both plots achieved satisfactory results, highlighting the advantages of integrating HLS and UAV-LS data for tree height estimation.

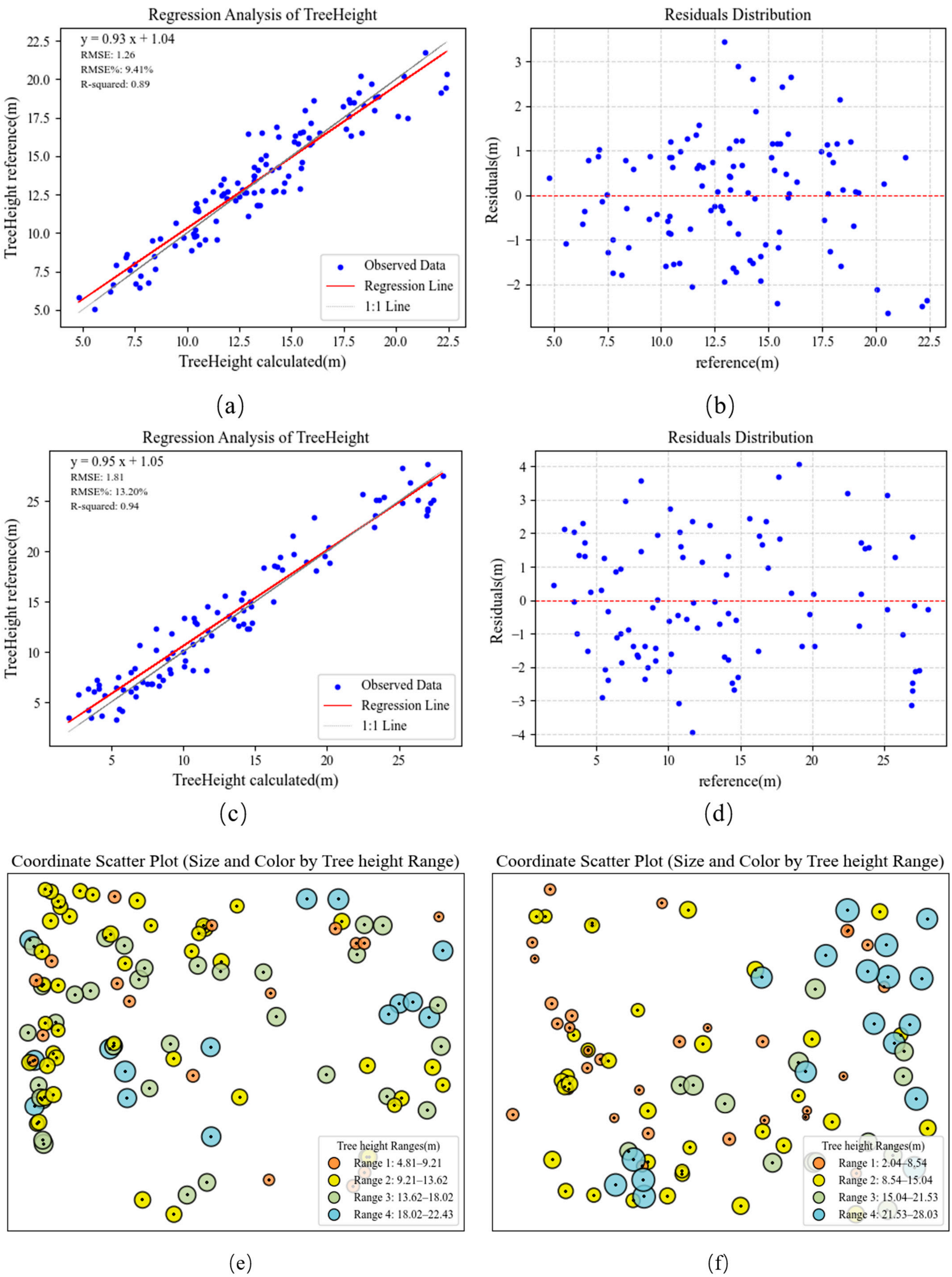

Figure 11. Comparison of extracted H_t with field-measured reference values for two plots, along with the distribution of calculated tree heights for plot 1 (**e**) and plot 2 (**f**). (**a**,**b**) show the extracted H_t values versus the reference values and corresponding residuals for Plot 1; (**c**,**d**) present the same comparison for plot 2.

4.1.3. Accuracy Analysis of Timber Volume

Figure 12 presents a detailed comparative analysis of timber volume estimates derived from the ABM method against the reference timber volume values calculated using the binary volume model for all individual tree point cloud datasets across two distinct plots. This evaluation provides critical insights into the precision and reliability of our ABM-based timber volume estimation approach. In plot 1 (Figure 12a), the RMSE for the estimated timber volume is 0.10 m^3, with the RMSE% of 34.65%, indicating a relatively low average discrepancy between predicted and actual volumes. The linear regression model yields a R^2 of 0.90, suggesting a strong positive linear correlation. Moreover, the CCC, which measures the agreement between the two datasets beyond mere correlation, is 0.95, reflecting a high degree of concordance. The slope of the fitted regression line is 0.83, indicating a slight underestimation trend relative to the reference values, though remaining within an acceptable range for practical applications.

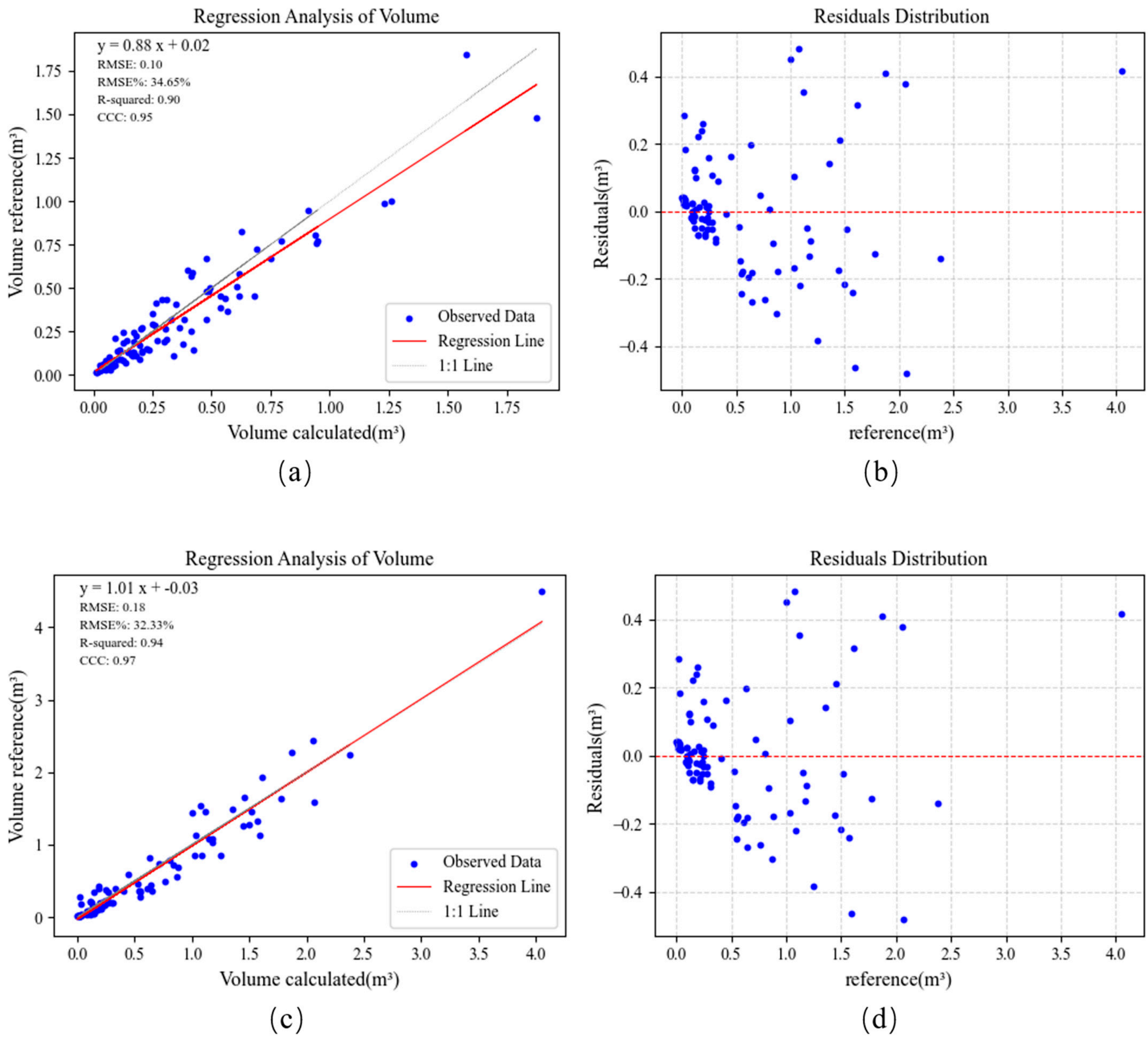

Figure 12. *Cont.*

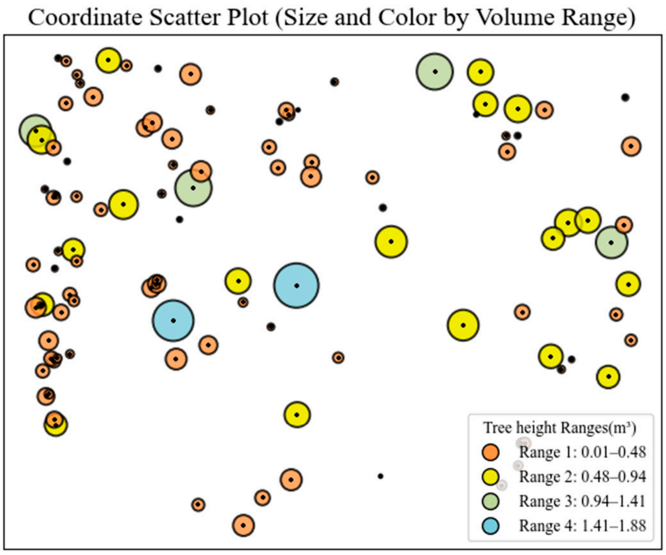

(e)

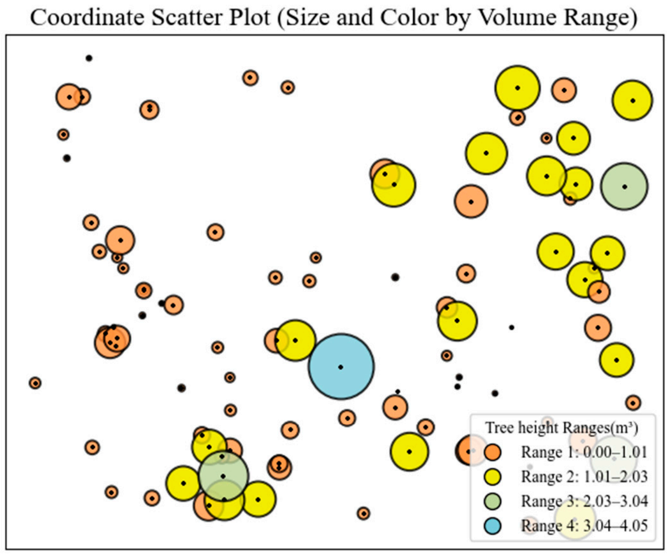

(f)

Figure 12. Comparison of timber volume estimates derived using the ABM method with those obtained from the binary volume model across two plots. (**a**,**b**) show the estimated individual tree volumes versus reference values and corresponding residuals for plot 1; (**c**,**d**) present the same comparison for plot 2. (**e**,**f**) illustrate the estimated individual tree volumes for plot 1 and plot 2, respectively.

In plot 2 (Figure 12c), the RMSE for the estimated timber volume increases to 0.18 m^3, with an RMSE% of 32.33%, suggesting a slightly higher average discrepancy compared to plot 1. However, the linear regression model still demonstrates a strong correlation, with an R^2 value of 0.94. The CCC for this plot is even higher at 0.97, indicating an exceptional level of agreement between the estimated and reference values. The slope of the fitted regression line is 1.01, closely approximating the ideal 1:1 relationship, which suggests that, on average, the ABM method provides accurate timber volume estimates in plot 2.

Examining the residual plots for both samples provides further nuance. In plot 1 (Figure 12c), the residuals (differences between estimated and reference values) range predominantly between -0.3 and 0.3 m^3, with only a few outliers beyond this interval. In plot 2 (Figure 12d), the residuals are slightly wider, spanning between -0.4 and 0.4 m^3, though still within a relatively narrow range. Notably, the residual values for timber volume estimation in both plots tend to increase as the timber volume itself increases. This trend may be attributed to the inherent challenges in accurately measuring larger volumes, where even minor errors in height or diameter estimates can have a more pronounced impact on the final volume calculation.

5. Discussion

5.1. DBH Estimation Accuracy and Influencing Factors

The DBH estimation accuracy in this study (R^2 = 0.89, RMSE% = 13.95% for plot 1; R^2 = 0.90, RMSE% = 14.75% for plot 2) was comparatively lower than previous research findings (R^2 up to 0.99) [14]. This discrepancy may be attributed to several factors. In our study, tree trunk DBH estimation primarily relied on circular fitting, which is sensitive to point cloud completeness. While some studies achieved R^2 values of 0.95–0.99 using ground-based point clouds alone [14,28], these were typically conducted in plantations or sparse forests with favorable conditions, enabling high-quality point cloud acquisition. Several factors may account for this discrepancy. In DBH estimation within forest plot, the estimation primarily relies on circular fitting of tree trunks. Some studies have established that forest plot DBH estimation does not depend on fused point cloud data but rather on ground-based point cloud data [28,37]. In previous studies, the plots for data acquisition were mostly located in natural or plantation forests with favorable environmental conditions, which allowed for the collection of high-quality point cloud data. In contrast, the plots in the present study were located in primary tropical rainforest on Hainan Island, characterized by a dense understory of shrubs and liana vegetation. These structural complexities posed challenges for ground-based LiDAR data acquisition, limiting visibility and reducing the completeness of trunk point clouds. Although both automated and manual noise removal procedures were applied after individual tree segmentation, residual occlusions and noise remained, ultimately reducing the accuracy of DBH estimation.

5.2. Tree Height Estimation and Multi-Source Data Integration

Tree height is a critical parameter for estimating volume of individual trees. Prior research has shown that tree height derived from a single point cloud source tends to be underestimated due to instrument limitations and environmental occlusion effects [14,38,39]. Integrating multi-source point cloud data effectively alleviates this problem. Since tree height is calculated from the highest normalized point after removing ground elevation, DEM accuracy directly impacts height estimation. In UAV-LS data acquisition, canopy occlusion often limits ground point detection, leading to DEM errors and tree height underestimation. Other influencing factors include point cloud sampling density, ground point extraction algorithms, terrain ruggedness, and vegetation type [40]. In regions with flat terrain and sparse vegetation, UAV-LS alone can typically capture sufficient ground points to generate highly accurate DEMs, however, this is not the case in more complex environments. On the other hand, using only ground-based equipment makes it difficult to accurately detect the highest point of individual trees. Study [14] indicated that using terrestrial LiDAR data alone yielded a maximum R^2 of only 0.39 for tree height estimation. According to Study [39], the R^2 values for individual tree height estimation using a handheld LiDAR scanner were 0.35 in subtropical secondary forests and 0.52 in primary forests. Therefore, in the study area of this research, the integration of multi-source point cloud data can effectively leverage the strengths of different systems and substantially improve the accuracy of tree height estimation.

In our experiments, R^2 values for tree height estimation reached 0.89 and 0.94 for plots 1 and 2, respectively. While slightly lower than results reported in plantations (R^2 = 0.96–0.98) [28] or sparse natural forests (R^2 = 0.98) [41], the performance demonstrates that meaningful estimation accuracy is achievable through multi-source data fusion, even in structurally complex rainforest environments.

5.3. Volume Estimation Bias and Modeling Limitations

Using the proposed method, individual tree volumes were estimated for both plots. The results revealed a strong correlation between the volumes computed using the ABM and those predicted by the binary volume model, indicating the reliability of the proposed approach (R^2 > 0.9). But there are some issues that exist, analysis of the residuals from tree volume estimation revealed that deviations increased proportionally with tree volume. Several factors contribute to this phenomenon. First, although the AdTree-based method is capable of effectively modeling trees, discrepancies remain between the reconstructed models and the actual tree morphology. In reality, tree trunks are rarely perfectly cylindrical, introducing more significant biases for larger trees [42]. Moreover, complete reconstruction of tree branches remains challenging [43]. As branch length increases, point cloud completeness diminishes along the growth direction, and reconstruction becomes nearly impossible at branch tips [43]. Previous studies have indicated that cylinder-fitting-based approaches are able to reconstruct only about 50% of the total branch length [44]. In tropical rainforests, trees—especially large individuals—tend to have more complex branching patterns, further amplifying modeling errors. Consequently, modeling larger trees tends to produce greater deviations in volume estimation.

5.4. Methodological Limitations and Uncertainty Sources

Our volume estimation method was validated against a binary volume model rather than through destructive sampling, introducing potential uncertainties. Since the study area is located in Hainan Tropical Rainforest National Park, destructive sampling is prohibited, preventing direct comparison between predicted and actual tree volumes. Previous studies have highlighted that only destructive sampling can provide a reliable ground-truth reference for validating tree volume estimates [45]. Even in previous studies, destructive sampling has rarely been conducted, as it is time-consuming, costly, and, in some cases, not permitted due to conservation policies [46,47].

Additionally, this study did not collect detailed species-level information, which introduces an additional limitation. Although the binary volume model used in this study has been validated with a large dataset, discrepancies may still exist for certain species with atypical growth patterns, where model-estimated volumes may deviate from actual tree volumes. Lastly, due to the highly complex environment of tropical rainforests, inevitable measurement errors may occur during field data collection. In particular, both systematic and random errors may arise during DBH and tree height measurements, caused by vegetation interference, canopy occlusion, and other environmental factors [48].

Nevertheless, despite these uncertainties, individual-tree-based modeling and volume estimation provide more precise and informative insights than area-based methods [49], thereby offering greater potential for carbon stock assessment, ecological monitoring, and forest management.

5.5. Challenges and Future Work

Previous studies on automated individual-tree parameter extraction have primarily focused on plantations or temperate coniferous forests, where homogeneous structures, regular spacing, and minimal canopy overlap facilitate data acquisition and processing. In contrast, tropical rainforests exhibit extreme structural complexity, including dense vegetation, overlapping canopies, irregular spacing, and diverse species compositions, which limit LiDAR penetration and accuracy. These challenges complicate downstream tasks such as ground point extraction and individual tree segmentation, highlighting the urgent need for more advanced, adaptive, and robust algorithms.

Future research should focus on several key directions to further improve the robustness and accuracy of individual-tree parameter estimation in complex tropical rainforest environments. First, the current study relies on positioning device outputs for dataset fusion and registration. However, in highly cluttered forest environments, positioning failures may occur, potentially reducing registration accuracy. To address this challenge, future studies should investigate feature-based registration approaches that utilize the intrinsic geometric and radiometric characteristics of multi-source point cloud data, thereby reducing dependence on external positioning devices.

Second, the modeling process in this study depends on individual tree point clouds obtained through segmentation of plot-level point clouds. However, existing individual tree segmentation algorithms often perform poorly under the structural complexity of tropical rainforests, where dense understory vegetation and canopy overlap hinder accurate boundary delineation. Future work should focus on developing more advanced, adaptive, and robust segmentation algorithms specifically designed for heterogeneous forest structures.

Finally, the ground-truth tree volumes used in this study were derived from a binary volume model, which inevitably introduces some degree of estimation bias. To further validate the applicability and accuracy of the proposed method, future studies should incorporate field experiments in sample plots where true tree volumes can be directly obtained through controlled destructive sampling or alternative high-precision techniques.

6. Conclusions

This study employs a 3D reconstruction approach (ABM) that synergizes AdTree and AdQSM algorithms to enable direct, non-destructive estimation of individual tree timber volumes from fused point cloud datasets. By integrating HLS and UAV-LS technologies, the methodology overcomes structural data acquisition challenges in complex tropical rainforest ecosystems, as demonstrated through field experiments in two natural forest plots on Hainan Island, China. The ABM approach achieves high-fidelity extraction of key structural parameters of DBH and tree height with RMSE of 2.93 cm and 1.26 m in plot 1, and 3.95 cm and 1.81 m in plot 2. Notably, the direct volumetric modeling from point clouds eliminates reliance on allometric equations, yielding RMSE values of 0.10 m^3 and 0.18 m^3 against binary volume model references, with R^2 of 0.90 and 0.94 for the two plots.

The fusion of HLS and UAV-LS data addresses critical limitations of single-source LiDAR systems, particularly in capturing below-canopy trunk details and above-canopy crown architecture, thereby enhancing structural data completeness and reducing occlusion-related inaccuracies. The ABM method demonstrated robust performance, even in plot 2, characterized by taller, more dispersed trees with larger diameters, despite higher residual variability attributed to measurement challenges in dense foliage. These findings highlight the method's adaptability to heterogeneous forest structures, where traditional survey techniques struggle with data incompleteness and labor intensity.

Author Contributions: Methodology, Z.C. and Z.L.; Software, D.D.; Validation, X.C.; Investigation, X.P., T.W. and Y.L.; Data curation, X.P.; Writing—original draft, Z.C.; Writing—review & editing, T.S.; Visualization, J.L.; Project administration, Z.C. and Y.C.; Funding acquisition, Y.C. All authors have read and agreed to the published version of the manuscript.

Funding: This work was financially supported by the Hainan Provincial Technical Innovation Program for Provincial Research Institutes (KYYSLK2023-016).

Data Availability Statement: The raw data supporting the conclusions of this article will be made available by the authors on request.

Conflicts of Interest: The authors declare no conflict of interest.

References

1. Bonan, G.B. Forests and climate change: Forcings, feedbacks, and the climate benefits of forests. *Science* **2008**, *320*, 1444–1449. [CrossRef]
2. Marchi, M.; Ferrara, C.; Bertini, G.; Fares, S.; Salvati, L. A sampling design strategy to reduce survey costs in forest monitoring. *Ecol. Indic.* **2017**, *81*, 182–191. [CrossRef]
3. Panagiotidis, D.; Abdollahnejad, A. Reliable Estimates of Merchantable Timber Volume from Terrestrial Laser Scanning. *Remote Sens.* **2021**, *13*, 3610. [CrossRef]
4. Blanchard, G.; Barbier, N.; Vieilledent, G.; Ibanez, T.; Hequet, V.; McCoy, S.; Birnbaum, P. UAV-Lidar reveals that canopy structure mediates the influence of edge effects on forest diversity, function and microclimate. *J. Ecol.* **2023**, *111*, 1411–1427. [CrossRef]
5. Tymen, B.; Réjou-Méchain, M.; Dalling, J.W.; Fauset, S.; Feldpausch, T.R.; Norden, N.; Phillips, O.L.; Turner, B.L.; Viers, J.; Chave, J. Evidence for arrested succession in a liana-infested Amazonian forest. *J. Ecol.* **2016**, *104*, 149–159. [CrossRef]
6. Puliti, S.; Dash, J.P.; Watt, M.S.; Breidenbach, J.; Pearse, G.D. A comparison of UAV laser scanning, photogrammetry and airborne laser scanning for precision inventory of small-forest properties. *Forestry* **2020**, *93*, 150–162. [CrossRef]

7. Yusup, A.; Halik, U.; Keyimu, M.; Aishan, T.; Abliz, A.; Dilixiati, B.; Wei, J.X. Trunk volume estimation of irregular shaped riparian forest using TLS point cloud data and multivariate prediction models. *For. Ecosyst.* **2023**, *10*, 100082. [CrossRef]
8. Lin, Y.; Jiang, M. A New Algorithm for MLS-Based DBH Mensuration and Its Preliminary Validation in an Urban Boreal Forest: Aiming at One Cornerstone of Allometry-Based Forest Biometrics. *Remote Sens.* **2018**, *10*, 749. [CrossRef]
9. Liu, G.J.; Wang, J.L.; Dong, P.L.; Chen, Y.; Liu, Z.Y. Estimating Individual Tree Height and Diameter at Breast Height (DBH) from Terrestrial Laser Scanning (TLS) Data at Plot Level. *Forests* **2018**, *9*, 398. [CrossRef]
10. Panagiotidis, D.; Surový, P.; Kuželka, K. Accuracy of Structure from Motion models in comparison with terrestrial laser scanner for the analysis of DBH and height influence on error behaviour. *J. For. Sci.* **2016**, *62*, 357–365. [CrossRef]
11. Cabo, C.; Del Pozo, S.; Rodríguez-Gonzálvez, P.; Ordóñez, C.; González-Aguilera, D. Comparing Terrestrial Laser Scanning (TLS) and Wearable Laser Scanning (WLS) for Individual Tree Modeling at Plot Level. *Remote Sens.* **2018**, *10*, 540. [CrossRef]
12. Panagiotidis, D.; Abdollahnejad, A. Accuracy assessment of total stem volume using close-range sensing: Advances in precision forestry. *Forests* **2021**, *12*, 717. [CrossRef]
13. Bu, G.C.; Wang, P. Adaptive circle-ellipse fitting method for estimating tree diameter based on single terrestrial laser scanning. *J. Appl. Remote Sens.* **2016**, *10*, 026040. [CrossRef]
14. Ruhan, A.; Du, W.L.; Ying, H.; Wei, B.C.; Shan, Y.; Dai, H.Y. Estimation of Aboveground Biomass of Individual Trees by Backpack LiDAR Based on Parameter-Optimized Quantitative Structural Models (AdQSM). *Forests* **2023**, *14*, 475. [CrossRef]
15. Chiappini, S.; Pierdicca, R.; Malandra, F.; Tonelli, E.; Malinverni, E.S.; Urbinati, C.; Vitali, A. Comparing Mobile Laser Scanner and manual measurements for dendrometric variables estimation in a black pine (Arn.) plantation. *Comput. Electron. Agric.* **2022**, *198*, 107069. [CrossRef]
16. Calders, K.; Newnham, G.; Burt, A.; Murphy, S.; Raumonen, P.; Herold, M.; Culvenor, D.; Avitabile, V.; Disney, M.; Armston, J.; et al. Nondestructive estimates of above-ground biomass using terrestrial laser scanning. *Methods Ecol. Evol.* **2015**, *6*, 198–208. [CrossRef]
17. Liu, L.L.; Zhang, A.W.; Xiao, S.; Hu, S.X.; He, N.P.; Pang, H.Y.; Zhang, X.Z.; Yang, S.K. Single Tree Segmentation and Diameter at Breast Height Estimation with Mobile LiDAR. *IEEE Access* **2021**, *9*, 24314–24325. [CrossRef]
18. Panagiotidis, D.; Abdollahnejad, A.; Slavík, M. 3D point cloud fusion from UAV and TLS to assess temperate managed forest structures. *Int. J. Appl. Earth Obs.* **2022**, *112*, 102917. [CrossRef]
19. Terryn, L.; Calders, K.; Bartholomeus, H.; Bartolo, R.; Brede, B.; D'hont, B.; Disney, M.; Herold, M.; Lau, A.; Shenkin, A. Quantifying tropical forest structure through terrestrial and UAV laser scanning fusion in Australian rainforests. *Remote Sens. Environ.* **2022**, *271*, 112912. [CrossRef]
20. Wu, Y.J.; Mao, Z.H.; Guo, L.J.; Li, C.R.; Deng, L. Forest Volume Estimation Method Based on Allometric Growth Model and Multisource Remote Sensing Data. *IEEE J.-Stars* **2023**, *16*, 8900–8912. [CrossRef]
21. Brede, B.; Calders, K.; Lau, A.; Raumonen, P.; Bartholomeus, H.M.; Herold, M.; Kooistra, L. Non-destructive tree volume estimation through quantitative structure modelling: Comparing UAV laser scanning with terrestrial LIDAR. *Remote Sens. Environ.* **2019**, *233*, 111355. [CrossRef]
22. Muumbe, T.P.; Tagwireyi, P.; Mafuratidze, P.; Hussin, Y.; van Leeuwen, L. Estimating above-ground biomass of individual trees with terrestrial laser scanner and 3D quantitative structure modelling. *South For.* **2021**, *83*, 56–68. [CrossRef]
23. de Tanago, J.G.; Lau, A.; Bartholomeus, H.; Herold, M.; Avitabile, V.; Raumonen, P.; Martius, C.; Goodman, R.C.; Disney, M.; Manuri, S.; et al. Estimation of above-ground biomass of large tropical trees with terrestrial LiDAR. *Methods Ecol. Evol.* **2018**, *9*, 223–234. [CrossRef]
24. Moorthy, S.M.K.; Raumonen, P.; Van den Bulcke, J.; Calders, K.; Verbeeck, H. Terrestrial laser scanning for non-destructive estimates of liana stem biomass. *For. Ecol. Manag.* **2020**, *456*, 117751. [CrossRef]
25. Du, S.L.; Lindenbergh, R.; Ledoux, H.; Stoter, J.; Nan, L.L. AdTree: Accurate, Detailed, and Automatic Modelling of Laser-Scanned Trees. *Remote Sens.* **2019**, *11*, 2074. [CrossRef]
26. Fan, G.P.; Nan, L.L.; Chen, F.X.; Dong, Y.Q.; Wang, Z.M.; Li, H.; Chen, D.Y. A New Quantitative Approach to Tree Attributes Estimation Based on LiDAR Point Clouds. *Remote Sens.* **2020**, *12*, 1779. [CrossRef]
27. Dong, Y.Q.; Fan, G.P.; Zhou, Z.W.; Liu, J.C.; Wang, Y.G.; Chen, F.X. Low Cost Automatic Reconstruction of Tree Structure by AdQSM with Terrestrial Close-Range Photogrammetry. *Forests* **2021**, *12*, 1020. [CrossRef]
28. Fekry, R.; Yao, W.; Cao, L.; Shen, X. Ground-based/UAV-LiDAR data fusion for quantitative structure modeling and tree parameter retrieval in subtropical planted forest. *For. Ecosyst.* **2022**, *9*, 100065. [CrossRef]
29. Melillo, J.M.; Mcguire, A.D.; Kicklighter, D.W.; Moore, B.; Vorosmarty, C.J.; Schloss, A.L. Global Climate-Change and Terrestrial Net Primary Production. *Nature* **1993**, *363*, 234–240. [CrossRef]
30. Dixon, R.K.; Brown, S.; Houghton, R.A.; Solomon, A.M.; Trexler, M.C.; Wisniewski, J. Carbon Pools and Flux of Global Forest Ecosystems. *Science* **1994**, *263*, 185–190. [CrossRef]
31. CloudCompare. Available online: https://cloudcompare.org/ (accessed on 26 August 2025).

32. Chetverikov, D.; Svirko, D.; Stepanov, D.; Krsek, P. The trimmed iterative closest point algorithm. In Proceedings of the 2002 International Conference on Pattern Recognition, Quebec City, QC, Canada, 11–15 August 2002; Volume 3, pp. 545–548. [CrossRef]
33. Tao, S.L.; Wu, F.F.; Guo, Q.H.; Wang, Y.C.; Li, W.K.; Xue, B.L.; Hu, X.Y.; Li, P.; Tian, D.; Li, C.; et al. Segmenting tree crowns from terrestrial and mobile LiDAR data by exploring ecological theories. *Isprs. J. Photogramm.* **2015**, *110*, 66–76. [CrossRef]
34. Zhao, X.Q.; Guo, Q.H.; Su, Y.J.; Xue, B.L. Improved progressive TIN densification filtering algorithm for airborne LiDAR data in forested areas. *Isprs. J. Photogramm.* **2016**, *117*, 79–91. [CrossRef]
35. West, G.B.; Brown, J.H.; Enquist, B.J. A general model for the structure and allometry of plant vascular systems. *Nature* **1999**, *400*, 664–667. [CrossRef]
36. Cheng, W.S.; Feng, Z.K.; Yu, J.G. Development of generic standard volume model and derived from factor model for major tree species in China. *Trans. Chin. Soc. Agric. Mach.* **2017**, *48*, 245–252.
37. Shimizu, K.; Nishizono, T.; Kitahara, F.; Fukumoto, K.; Saito, H. Integrating terrestrial laser scanning and unmanned aerial vehicle photogrammetry to estimate individual tree attributes in managed coniferous forests in Japan. *Int. J. Appl. Earth Obs.* **2022**, *106*, 102658. [CrossRef]
38. Laurin, G.V.; Ding, J.; Disney, M.; Bartholomeus, H.; Herold, M.; Papale, D.; Valentini, R. Tree height in tropical forest as measured by different ground, proximal, and remote sensing instruments, and impacts on above ground biomass estimates. *Int. J. Appl. Earth Obs.* **2019**, *82*, 101899. [CrossRef]
39. Mak, N.P.L.; Siu, T.Y.; Law, Y.K.; Zhang, H.; Sui, S.T.; Yip, F.T.; Ng, Y.S.; Ye, Y.H.; Cheung, T.C.; Wa, K.C.; et al. Mapping Individual Tree- and Plot-Level Biomass Using Handheld Mobile Laser Scanning in Complex Subtropical Secondary and Old-Growth Forests. *Remote Sens.* **2025**, *17*, 1354. [CrossRef]
40. Cateanu, M.; Ciubotaru, A. The Effect of LiDAR Sampling Density on DTM Accuracy for Areas with Heavy Forest Cover. *Forests* **2021**, *12*, 265. [CrossRef]
41. Rodda, S.R.; Nidamanuri, R.R.; Mayamanikandan, T.; Rajashekar, G.; Jha, C.S.; Dadhwal, V.K. Non-Destructive Allometric Modeling for Tree Volume Estimation in Tropical Dry Deciduous Forests of India Using Terrestrial Laser Scanner. *J. Indian Soc. Remote* **2024**, *52*, 825–839. [CrossRef]
42. Nogueira, E.M.; Nelson, B.W.; Fearnside, P.A. Volume and biomass of trees in central Amazonia: Influence of irregularly shaped and hollow trunks. *For. Ecol. Manag.* **2006**, *227*, 14–21. [CrossRef]
43. Cai, S.S.; Zhang, W.M.; Zhang, S.H.; Yu, S.S.; Liang, X.L. Branch architecture quantification of large-scale coniferous forest plots using UAV-LiDAR data. *Remote Sens. Environ.* **2024**, *306*, 114121. [CrossRef]
44. Liang, X.L.; Wang, Y.S.; Pyörälä, J.; Lehtomäki, M.; Yu, X.W.; Kaartinen, H.; Kukko, A.; Honkavaara, E.; Issaoui, A.E.I.; Nevalainen, O.; et al. Forest in situ observations using unmanned aerial vehicle as an alternative of terrestrial measurements. *For. Ecosyst.* **2019**, *6*, 20. [CrossRef]
45. Disney, M.I.; Vicari, M.B.; Burt, A.; Calders, K.; Lewis, S.L.; Raumonen, P.; Wilkes, P. Weighing trees with lasers: Advances, challenges and opportunities. *Interface Focus* **2018**, *8*, 20170048. [CrossRef]
46. Burt, A.; Vicari, M.B.; da Costa, A.C.L.; Coughlin, I.; Meir, P.; Rowland, L.; Disney, M. New insights into large tropical tree mass and structure from direct harvest and terrestrial lidar. *R. Soc. Open Sci.* **2021**, *8*, 201458. [CrossRef]
47. Abegg, M.; Bösch, R.; Kükenbrink, D.; Morsdorf, F. Tree volume estimation with terrestrial laser scanning-Testing for bias in a 3D virtual environment. *Agric. For. Meteorol.* **2023**, *331*, 109348. [CrossRef]
48. Wang, Y.S.; Pyörälä, J.; Liang, X.L.; Lehtomäki, M.; Kukko, A.; Yu, X.W.; Kaartinen, H.; Hyyppä, J. In situ biomass estimation at tree and plot levels: What did data record and what did algorithms derive from terrestrial and aerial point clouds in boreal forest. *Remote Sens. Environ.* **2019**, *232*, 111309. [CrossRef]
49. Muumbe, T.P.; Singh, J.; Baade, J.; Raumonen, P.; Coetsee, C.; Thau, C.; Schmullius, C. Individual Tree-Scale Aboveground Biomass Estimation of Woody Vegetation in a Semi-Arid Savanna Using 3D Data. *Remote Sens.* **2024**, *16*, 399. [CrossRef]